

RAWDET-7: A Multi-Scenario Benchmark for Object Detection and Description on Quantized RAW Images

Mishal Fatima^{1*}, Shashank Agnihotri^{1*}, Kanchana Vaishnavi Gandikota²,
Michael Moeller², Margret Keuper^{1,3}

¹University of Mannheim, Germany ²University of Siegen, Germany

³Max Planck Institute for Informatics, Saarland Informatics Campus, Germany

Abstract

Most vision models are trained on RGB images processed through ISP pipelines optimized for human perception, which can discard sensor-level information useful for machine reasoning. RAW images preserve unprocessed scene data, enabling models to leverage richer cues for both object detection and object description, capturing fine-grained details, spatial relationships, and contextual information often lost in processed images. To support research in this domain, we introduce RAWDET-7, a large-scale dataset of $\sim 25k$ training and $7.6k$ test RAW images collected across diverse cameras, lighting conditions, and environments, densely annotated for seven object categories following MS-COCO and LVIS conventions. In addition, we provide object-level descriptions derived from the corresponding high-resolution sRGB images, facilitating the study of object-level information preservation under RAW image processing and low-bit quantization. The dataset allows evaluation under simulated 4-bit, 6-bit, and 8-bit quantization, reflecting realistic sensor constraints, and provides a benchmark for studying detection performance, description quality & detail, and generalization in low-bit RAW image processing. Dataset & code upon acceptance.

1. Introduction

Most vision pipelines operate on standard RGB (sRGB) images with 8-bit depth. During image capture, however, cameras record visual information in a much higher bit-depth (~ 24 -bit) RAW format, which is then converted to sRGB by an image signal processor (ISP). This conversion involves a sequence of steps, including black-level subtraction, demosaicking, denoising, white balancing, gamma correction, color correction, and compression, and is usually conceived

to produce a visually pleasing 8-bit color image. However, this photography-oriented imaging pipeline is not optimized for downstream vision tasks. Compared with processed sRGB images, RAW images contain more precise sensor measurements, preserving the full bit depth and dynamic range. Leveraging RAW data for downstream tasks can therefore improve performance [31, 40]. RAW data, however, varies significantly across camera sensors, each of which may use different bit depths and ISP pipelines to produce sRGB images. As a result, for specialized applications [1, 18, 36], jointly optimizing the imaging hardware or ISP pipeline together with the downstream task can be beneficial. Despite these potential advantages, progress in using RAW data and end-to-end learned, task-specific image processing remains constrained by the limited availability of large-scale, well-annotated RAW datasets.

To address this, we introduce RAWDET-7, a comprehensive dataset for object detection and description on RAW images. We chose the task of object detection as it requires both identifying and localizing features associated with objects of specific classes within images. Furthermore, we provide a curated subset of sRGB images accompanied by object descriptions, specifically designed to assist researchers in evaluating the level of detail preserved in processed RAW images. The proposed RAWDET-7 has a larger sample size than all previous datasets, comprising $\sim 25k$ training and $\sim 7.6k$ test images obtained by consolidating four different datasets [16, 29, 31, 40] across varied lighting conditions, camera types, and environments. As many prior datasets have only a few object classes, typically covering only large prominent objects, we derive more fine-grained labels by relabeling the consolidated dataset using a large foundation model with subsequent human validation on the sRGB versions of the RAW images to annotate 7 object categories, that align with community accepted naming conventions from MS-COCO [23] and LVIS [14] datasets. As a result, the proposed dataset provides denser annotations, both in terms of increasing the number of ob-

*These authors contributed equally to this work.

Emails: mishal.fatima@uni-mannheim.de, shashank.agnihotri@uni-mannheim.de

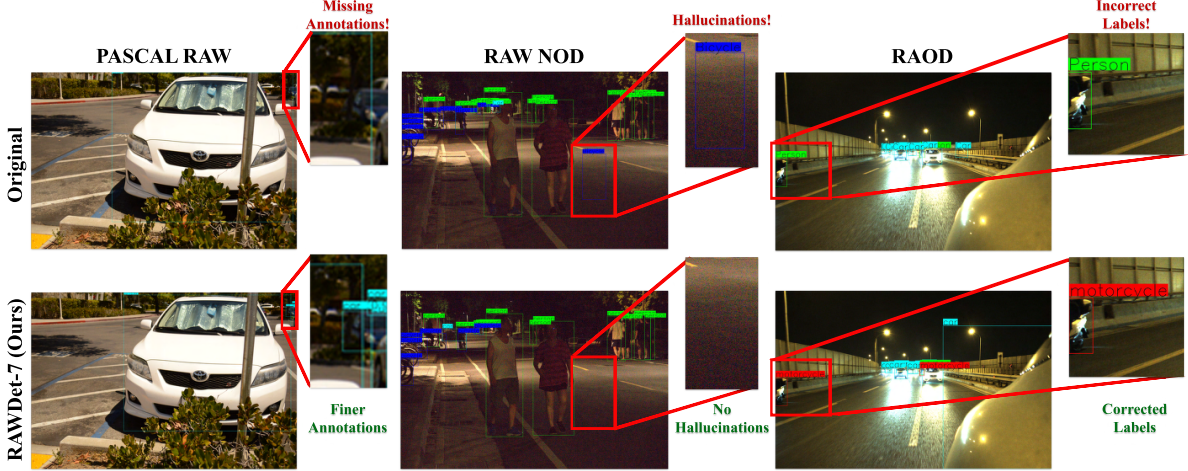


Figure 1. Comparing ground truth annotations provided in the original datasets and the new ones proposed in RAWDET-7. Our proposed annotations are more fine-grained, as seen for PASCAL RAW, which originally annotated only one instance of the cars in the image; we now annotate all the other instances of cars in the image (with a 20% overlap threshold i.e. at least 20% area of the bounding box should be non-overlapping). RAW NOD (-Nikon and -Sony), RAOD (-Day and -Night) original annotations contain hallucinations as seen here for RAW NOD, which hallucinates a bicycle in the center right of the frame. Original annotations even contain some misclassifications, as seen for RAOD, which misclassified a motorcycle as a person. RAWDET-7 (**bottom**) **overcomes these drawbacks**.

ject categories and improving the annotation of small and occluded instances, which significantly enhances the utility of the proposed dataset, RAWDET-7, in developing robust detection models that generalize to real-world scenarios. This can be observed in Fig. 1, RAWDET-7 has significantly richer and corrected annotations than previous datasets for the same images. While RAWDET-7 comprises full-precision RAW images, reducing the bit depth has shown benefits in memory consumption and significant power gains [43]. However, there is limited knowledge on the performance of complex downstream vision methods on heavily quantized RAW input. Thus, we benchmark the performance of object detection models under simulated low-bit quantization, in addition to sRGB images.

We consider low-bit quantized inputs obtained using different information processing methods: linear scaling, logarithmic scaling [4], learnable γ scaling [28], and a combination of logarithmic and learnable γ scaling [11]. Through analytical benchmarking of object detection methods low-bit quantized RAW inputs, we demonstrate that models trained on the proposed RAWDET-7 have an improved object detection performance over models trained on the individual subsets across different quantization levels, with more robust detections on small and occluded instances, demonstrating the benefit of the proposed dataset. Moreover, note that all prominent object detection methods proposed, including every design decision made, were optimized for sRGB input. We show in our benchmarking that, despite this obvious bias, object detection methods trained on RAW input, especially low-bit RAW input, with input scaling can perform at-par with (sometimes even surpass)

their counterparts trained on the same amount of sRGB input. We also evaluate the fidelity of processed RAW images by comparing the object descriptions obtained from different scaling variants with the ground truth captions generated from high-resolution sRGB images. Our results suggest that descriptions generated from processed RAW images exhibit greater similarity to those from high-resolution sRGB images and provide more accurate explanations of objects compared than captions from linear RAW images.

The contributions of this work are as follows:

- We introduce a comprehensive dataset for object detection on RAW images, designed to support research in low-bit quantized sensing from RAW data.
- We analytically benchmark object detection models on RAW images quantized to different bit depths using four input scaling methods.
- We demonstrate that RAW images quantized to as low as 4 bits can perform on-par or better than the models trained on standard 8-bit RGB images.
- We demonstrate the utility of our large-scale dataset in improving the performance of object detection models across different sensors, lighting conditions, and bit depths compared to the individual datasets.
- By providing object-level descriptions for a subset of images derived from high-resolution sRGB images, we create a ground truth reference that can be used to evaluate captions generated from other image representations.
- Lastly, we show that the observed benefits of RAWDET-7 and input scaling methods are not limited to traditional object detection methods but also extend to recent large foundational model-based object detection methods.

2. Related Work

In the following, we discuss prior works towards object detection on RAW images, and relevant RAW image datasets that align closely with the proposed RAWDET-7.

Object detection. We rely on established object detection architectures to benchmark and analyze performance on RAW and quantized RAW image formats. **Faster R-CNN** [32] serves as a strong two-stage baseline, leveraging region proposal networks for object localization. To assess performance under a one-stage paradigm, we include **RetinaNet** [24], which uses focal loss to address class imbalance, and **PAA** [17], which adaptively selects positive samples through probabilistic anchor assignment. These models are widely used in both academic and industrial settings due to their strong performance and robustness across a variety of detection benchmarks. Finally, to evaluate whether our observations generalize to more recent and large-scale detection architectures, we also include **MM-Grounding DINO** [45], a foundation model for open-set object detection that we employ in a frozen setting. We use this diverse set of methods to enable a broad and representative analysis of detection performance in the RAW image domain.

RAW Imaging Datasets. Most existing datasets and models for object detection are developed on RGB images produced by ISP pipelines optimized for human perception. In contrast, RAW images preserve richer scene information and higher dynamic range, which may benefit high-level tasks such as detection [28, 39, 40]. However, large-scale annotated RAW datasets remain scarce. Existing detection datasets like RAOD [40], NOD [29], MultiRAW [22] and PASCAL RAW [31] are limited in either the number of images, object classes, or annotation quality, PASCAL RAW annotates only large objects, NOD and RAOD contain hallucinated or noisy labels, and all three cover a narrow range of conditions. The Zurich dataset [16], originally designed for RAW-to-RGB ISP learning, lacks detection labels and is re-annotated in our work. Other RAW datasets [9, 16, 35] focus on ISP or forensics, not object detection.

To address these limitations, prior works propose synthetic RAW data generation [21, 44] or task-adaptive ISP modules [8, 10, 30, 33] for improving detection. Some methods [4, 40] evaluate the effect of low-bit quantization on recognition but do not optimize quantization-aware pipelines, while others [25, 28] jointly learn simplified ISPs with detection models. In contrast, our proposed dataset, RAWDET-7, unifies and re-annotates existing datasets with fine-grained labels for seven categories across varied lighting, sensor types, and scenes, and enables controlled benchmarking under realistic 4-bit, 6-bit, and 8-bit quantization. For evaluation, we adopt standard detectors including Faster R-CNN [32], RetinaNet [24], and PAA [17], as well as MM-Grounding DINO [45], demonstrating that our findings gen-

eralize across architectures and detection paradigms.

Object Description. Recent works have explored set-of-mark and visual prompting strategies to improve region-level grounding and object-centric captioning in large vision-language models [5, 20, 38, 41, 42]. Set-of-Mark prompting overlays alphanumeric marks and segmentation-derived regions so that a VLM can reason about specific objects and their relations directly on the image [41]. [38] instead compares predictions on images with highlighted versus blacked-out regions to reduce prior biases and better follow region prompts. [20] introduces a coordinate grid on the image together with textual references to enhance spatial reasoning and vision-language coordination. ViP-LLaVA [5] trains multimodal models to interpret arbitrary user-drawn prompts such as boxes, arrows, and scribbles as region selectors, while [42] uses precise segmentation masks and blur-outside-mask operations to focus the model on a target instance. In RAWDET-7, we adopt a set-of-marks interface and additionally provide a high-level object class for each numeric mark when prompting the VLM, allowing us to study how well detailed object descriptions are preserved across different quantizations.

3. Proposed Dataset RAWDET-7

RAWDET-7 provides high quality annotations for object detection as well as for object description. The following sections provide the details of the annotation process.

3.1. Detection Annotations

As discussed in Sec. 1, RAW images have been underutilized in research due to a lack of large-scale, high-quality benchmarks and the practical challenges of managing RAW data. Although several RAW object detection datasets [29, 31, 40] have been proposed in the literature, we discuss in Sec. 2 that these datasets have practical limitations. For instance, PASCAL RAW [31] and NOD [29] focus on only a few coarse object classes, limiting object categories to ‘Car’, ‘Person’, and ‘Bicycle’. In Fig. 1 we observed several missing annotations even among these classes for small or partially occluded people and vehicles. NOD dataset [29] suffers from hallucinations and missing annotations, e.g., one could observe in Fig. 1 that a motorcycle (‘vehicle’ in the original category) from the RAOD [40] dataset is being mislabeled as a ‘Person’. Apart from the errors and missing annotations, sensor-specific differences in bit depth and lighting conditions introduce significant variability, captured only partially by previous datasets. Notably, MultiRAW [22] attempted increasing the number of classes and scenarios, but it has contradictory classes like ‘rider’ and ‘person’ and too few total samples making the problem complex.

To address these gaps, we introduce RAWDET-7, a comprehensive benchmark dataset for object detection on RAW

Table 1. Comparison of RAWDET-7 with other Datasets. Please refer to the Appendix for a more detailed comparison.

Dataset	Train Images	Test Images	# Classes	Bit Depth	Scenarios	# Sensors
PASCAL RAW	2128	2130	3	12-bit	Day	1
RAW NOD (ROD)	6692	1671	3	14-bit	Night	2
RAOD	16089	4000	5	24-bit	Day and Night	1
MultiRAW	5154	2315	10	10, 12, 14, 24-bit	Day and Night	5
RAWDET-7 (Ours)	24864	7688	7	10, 12, 14, 24-bit	Day and Night	5

images. Comprising over 32k RAW images of which there are 25k images for training and 7.6k for testing, RAWDET-7 consolidates and standardizes four existing datasets: PASCAL RAW [31] (12-bit depth), RAOD [40] (24-bit depth), covering day and night scenes in HDR format, Zurich RAW dataset [16] (10-bit depth), NOD dataset [29] (14-bit depth) containing data from Sony and Nikon sensors. These sources cover a wide range of imaging conditions, including daytime, nighttime, and high dynamic range (HDR) scenes, as well as diverse hardware and sensor bit depths. We unify these disparate datasets under a consistent annotation scheme, thereby enabling controlled studies of model generalization across lighting, scene complexity, and sensor variability. A key contribution of RAWDET-7 is its improved and standardized labeling. To remedy the deficiencies in annotations in the individual datasets, and to enable a uniform standardized annotation, we re-annotated all datasets using Grounded-DINO 1.5 [26] (paid API version at: https://deepdataspace.com/request_api) for seven object categories: ‘Car’, ‘Truck’, ‘Tram’, ‘Person’, ‘Bicycle’, ‘Motorcycle’, and ‘Bus’ following MS-COCO and LVIS-style naming conventions, and further refined the annotations produced by Grounded-DINO 1.5 by selecting confident annotations above the confidence threshold of 0.8. The cut-off threshold was chosen after manual inspection of the annotation quality and accuracy over a large subset of RAWDET-7. As a result, RAWDET-7 has dense annotations with uniform, high-quality labeling standards across the combined dataset with improved labeling of small and occluded object instances. The statistics of individual object categories in the consolidated dataset, as well as the individual subsets, are provided in Fig. 13. Tab. 4 lists the properties of individual subsets of RAWDET-7.

3.2. Object Description

While being precise in terms of localization, object detections only provide a coarse, class-level understanding of objects in a scene. To evaluate the level of detail preserved in processed RAW images, in particular on the highly relevant, annotated object categories, we propose to consider the task of *object description*. To this end, we generate a set of high-quality, detailed object descriptions using the Gemini-2.5-Pro model [7] for objects localized by the ground truth bounding box annotations from RAWDET-7. Specifically,

we overlay, for a subset of 500 high-resolution sRGB images, visual marks on annotated objects, in line with the procedure outlined in [41], using black, squared marks with colored numbers indicating the object ID. We then prompt Gemini-2.5-Pro to provide detailed descriptions for every object. To provide a reference, we prompt the model twice per image, thereby generating an upper bound on description agreement. Our full prompts and examples of object descriptions are provided in the appendix, along with the user study for dataset validation.

For evaluation, we calculate the RegeX overlap and BLeU score between captions generated for the high-resolution sRGB image, and downsampled sRGB variants and differently processed RAW variants of different bit-depths, for the same set-of-marks. Additionally, using Gemini-2.5-Flash-Lite as a judge (score 1-10), we calculate the semantic similarity (disregarding details), level of detail in caption (disregarding similarity), and the match in precise details of the pair of captions (sRGB and variant).

4. Scaling Methods Used For Benchmarking

One key challenge with using RAW images in machine learning is that their high precision and large size, make them computationally expensive to store and process. Quantization offers a practical solution by reducing bit depth, but it introduces new design choices around how to scale inputs before quantization. As an example use-case, in this section, we explore combinations of quantization with known input scaling methods, such as logarithmic and gamma mappings, to enable efficient and effective object detection directly on low-bit RAW inputs. Recording at lower bit-depth and skipping the ISP before feeding images to a downstream task model can provide power and memory gains [43], making such methods practical in scenarios like low-bandwidth or low-power consumption sensing.

We benchmark the performance of RAWDET-7 using low-bit depth images obtained using the following scaling methods, where \mathcal{X} with bit-depth N is the input to the quantizer $\mathcal{Q}(\cdot)$, which provides output with target bit depth \hat{N} :

1. **Linear quantization** converts input into a quantized digital value using uniform linear steps as

$$\mathcal{Q}(\mathcal{X}) = \left\lfloor \mathcal{X}_{\text{norm}} \cdot (2^{\hat{N}} - 1) \right\rfloor, \quad (1)$$

where, $\mathcal{X}_{\text{norm}} = \left(\frac{\mathcal{X}}{2^N - 1} \right)$ is the normalized version of \mathcal{X} . This naïve approach of reducing the bit-depth often fails, motivating better methods for scaling.

2. **Logarithmic quantization** proposed by [3, 4] non-linearly scales the dynamic range of \mathcal{X} before quantization,

$$\mathcal{Q}(\mathcal{X}) = \left\lfloor \frac{\mathcal{X}_{\log} - \min(\mathcal{X}_{\log})}{\max(\mathcal{X}_{\log}) - \min(\mathcal{X}_{\log})} \cdot (2^{\hat{N}} - 1) \right\rfloor, \quad (2)$$

where, $\mathcal{X}_{\log} = \log(\mathcal{X} + \epsilon)$, with ϵ is accounting for the mapping to issue values $\mathcal{X}_{\log} \geq 0$, i.e., [4] use $\epsilon = 1$.

3. **Quantization with Learnable γ -Scaling:** γ mapping, similar to logarithmic quantization, also compresses the dynamic range of the input, and we consider a learnable γ mapping before quantization as

$$\mathcal{Q}(\mathcal{X}, \gamma) = \left\lfloor \mathcal{X}_{\text{norm}}^{\gamma} \cdot (2^{\hat{N}} - 1) \right\rfloor, \quad (3)$$

where $\mathcal{X}_{\text{norm}}$ is the normalized version of \mathcal{X} as defined earlier in linear quantization, and the parameter γ is learned along with the parameters θ of the neural network. In addition to learning a single γ for the dataset, we also evaluate conditioning γ on the domain, such as lighting conditions or sensors. $\mathcal{Q}(\mathcal{X}, \gamma)$ is hereby referred to as γ -SCALING.

4. Since various non-linear mappings of input intensities are an active area of research for the sensors community [13, 19], we benchmark a combination of logarithmic and learned γ quantization. That is, we use $\mathcal{X}_{\text{norm}} = \mathcal{X}_{\log}$ in Eq. (3).

4.1. Learning Task-specific Low-bit Quantization

We learn the parameter γ of γ -SCALING and ‘Log + γ -SCALING’ jointly with the neural network parameters for the specific task by optimizing

$$\min_{\theta, \gamma} \mathbb{E}_{(\mathcal{X}, y)} [\mathcal{L}(\eta(\mathcal{Q}(\mathcal{X}, \gamma)), y; \theta)], \quad (4)$$

where η is the task-specific neural network with parameters θ , and where \mathcal{L} is a suitable loss function comparing the network output and the ground truth prediction y .

Since RAWDET-7 offers a unique multi-scenario optimization setting, we capitalize, and attempt learning γ values for different scenarios. Using one γ value over the entire dataset is denoted as 1- γ . When using two γ value we denote it as 2- γ , with the intention of them conditioning to the time of day, i.e. one γ for daytime and one for nighttime images. Lastly, we test using five γ values, denoted as 5- γ , allowing one optimized to each sensor.

For optimization, since the quantization operation stops the flow of gradients in the backward pass, we use a straight-through estimator to allow gradient-based optimization of

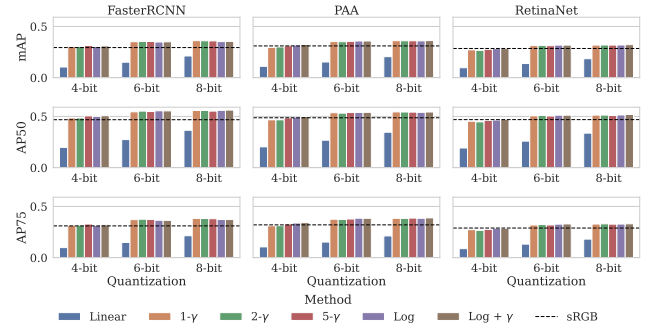


Figure 2. Benchmarking performance on RAWDET-7. Baselines such as logarithmic quantization and jointly learnt γ improve results across quantization levels and architectures.

γ . Please note that $\gamma < 0$ would lead to undesirable behavior, i.e., $\mathcal{X}_{\text{Q}} \geq 2^{\hat{N}} - 1$ when $N \geq \hat{N}$ (which is the case when we want to quantize to lower bit depths). To avoid this, we clamp γ to be non-negative, using $\text{ReLU}(\cdot)$ [12]. To take into account Bayer patterned images in the RAW dataset, we extract red, green, and blue channels from the Bayer patterned image and downsample it using nearest neighbor interpolation to simulate the capture of a low-resolution, low-bit-depth image, which is provided as input to the neural network. This pipeline for joint training of γ and task-specific neural network parameters θ using quantized RAW images is the methodology for the forthcoming evaluations.

5. Experiments

For object detection we use the mmdetection [6] framework from openmmlab. Following previous works [31, 40] that perform object detection on RAW images, we conduct experiments using three architectures Faster-RCNN [32], RetinaNet [24], and PAA [17] models with a pre-trained ResNet50 [15] backbone. For fair comparison with sRGB counterpart, we extract the ‘R’(Red), ‘G’ (Green), and ‘B’(Blue) channels from the Bayer patterned RAW input, average over the two ‘G’ channels and report the following quantitative evaluation metrics: mean average precision (mAP) is calculated by averaging the Average Precision (AP) values across the intersection over union (IoU) thresholds ranging from [0.5, 0.95] with a step size of 0.05, resulting in 10 threshold values. We also report performance with IoU-thresholds of 0.5 and 0.75 (AP50 and AP75) for each case. We use an ImageNet-1k [34] pretrained backbone and freeze the first stage of the backbone during training. We follow the multi-scale training setup commonly used [24, 32], during training, and at test time, the shorter edge length is kept at 800. We use a batch size of 16 and train the model for 140 epochs. We use SGD with Nesterov Momentum [37] as the optimizer with a weight decay of $1e^{-3}$. For the PASCAL RAW dataset, we use the same

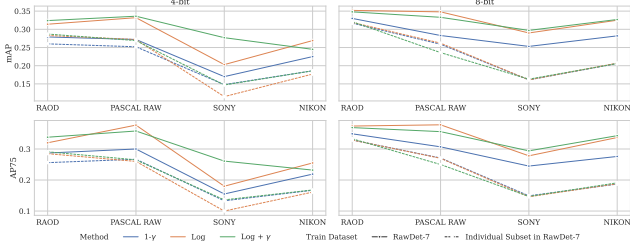


Figure 3. Results for training on combined RAWDET-7 when evaluated on each subset, vs. training only on a subset and evaluated the subset’s test set. Combining improves results on all subsets. The model used is Faster RCNN.

train/test split as proposed by the original paper. For the Nikon, Sony, and Zurich datasets, we do an 80-20 train/test split of the entire dataset. For RAOD, we use the publicly available validation set as the test set. All dataset splits and statistics are provided in Fig. 13, whereas their sensor models are provided in Tab. 4 in the appendix.

5.1. Benchmarking Performance on RAWDET-7

We report the performance of various object detection networks in the proposed RAWDET-7 benchmark, for different quantization levels in Fig. 2. Here we observe that naïvely reducing the bit depth through linear scaling and quantization to a low bit depth degrades the quality of fine-grained details that are critical for tasks like object detection. In comparison, the non-linear scaling and quantization methods perform significantly better at all the bit depths. Optimizing only a single additional parameter γ (for γ -scaling) jointly with the downstream network during training, we observe a significant improvement in detection performance over using both linearly scaled and quantized inputs, and sRGB inputs. This shows that even a lightweight, task-aware mapping of the input for quantization can lead to meaningful improvements over naïve quantization pipelines. Logarithmic scaling and quantization, albeit fixed, performs on par with or better than learned γ scaling. Among the different target bit depths considered, we observe that 4-bit linear scaling and quantization performs worse across all architectures. Improvements are observed by applying a logarithm or the learned γ scaling before the quantization. The improvements are on par with the sRGB setting, indicating that a simple baseline (such as log or learned γ), when applied before the quantization, alleviates the need for an ISP. We also learn separate γ during training for day and night images as well as separate γ for different sensors indicated by 2- γ and 5- γ , respectively in Fig. 2. We observe a marginal difference in performance while training with multiple γ values, while combining logarithmic scaling with learned γ scaling provides some gain in detection performance when compared to solely using logarithmic scaling for networks trained from scratch.

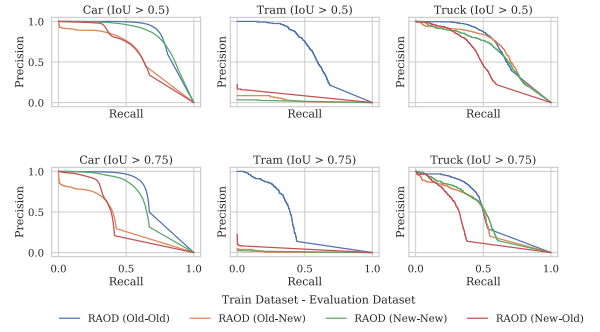


Figure 4. Precision Recall Curves for RAOD. “Old” refers to the annotations as proposed in the original dataset, whereas “New” means the annotations in RAWDET-7. All the models are trained on FasterRCNN, for 8-bit quantization and jointly learnt with 1 gamma. As mentioned in the legend, the keys are “(Train Dataset - Evaluation Dataset)”.

Table 2. Experiments with large VLM, MM-Grounding-DINO [45] with a Swin-T [27] backbone. For experiments with γ -SCALING and Log + γ -SCALING we finetune only the γ -SCALING parameter while keeping the VLM frozen, for the other methods, we evaluate zero-shot.

Quantization	Method	mAP	AP50	AP75	AP95
RGB	sRGB	0.188	0.215	0.204	0.088
	Linear	0.047	0.060	0.053	0.008
	Log	0.114	0.138	0.127	0.034
	γ -SCALING	0.104	0.125	0.115	0.035
4-bit RAW	Log + γ -SCALING	0.135	0.161	0.149	0.048
	Linear	0.066	0.081	0.074	0.014
	Log	0.149	0.182	0.164	0.042
	γ -SCALING	0.177	0.206	0.193	0.072
6-bit RAW	Log + γ -SCALING	0.198	0.230	0.217	0.085
	Linear	0.074	0.091	0.083	0.017
	Log	0.151	0.186	0.167	0.041
	γ -SCALING	0.177	0.207	0.193	0.070
8-bit RAW	Log + γ -SCALING	0.202	0.233	0.220	0.090
	Linear	0.075	0.092	0.084	0.017
	Log	0.152	0.187	0.168	0.041
	γ -SCALING	0.167	0.196	0.183	0.066
12-bit RAW	Log + γ -SCALING	0.201	0.232	0.219	0.089
	Linear	0.075	0.092	0.084	0.017
	Log	0.152	0.187	0.168	0.041
	γ -SCALING	0.167	0.196	0.183	0.066

5.2. Added Value by the Contributed Annotations

Fig. 4 shows the precision-recall curves for the RAOD dataset in four different settings. “Old-Old” means that the model was trained with original annotations and tested with them as well, whereas “Old-New” indicates a different test setting, testing with newly proposed annotations, and likewise for “New-New” and “New-Old”. Since the annotations in both cases are slightly different, we only compute the precision-recall curves for 4 mutually common annotations i.e. ‘Car’, ‘Tram’, ‘Truck’, and ‘Person’. We observe that the precision when tested with new annotations is lower for the same recall value. This indicates that the difficulty level of these annotations is higher compared to the original dataset. Fig. 3 shows that training on the proposed



Figure 5. Visualizing predictions made by MM-Grounding-DINO on RAWDET-7 at 6-bit quantization, using different methods for predictions on sRGB images and the expected Ground Truth predictions. Here for methods γ and $\text{Log} + \gamma$, we finetune only the γ parameter while keeping the VLM frozen; for the other methods, we evaluate zero-shot. We randomly sample three distinct scenarios to demonstrate the versatility of the proposed RAWDET-7.

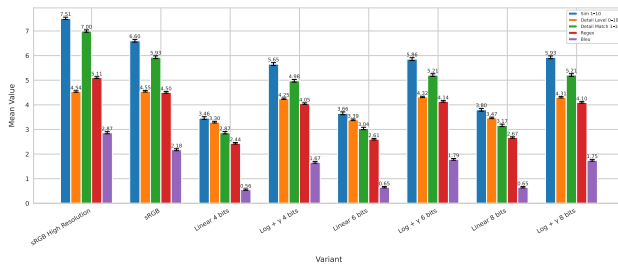


Figure 6. Object Description quality across different image variants. Descriptions are generated from linear and $\log + \gamma$ variants of quantized images using Gemini, with reference captions obtained from higher-resolution sRGB images. Here, sRGB refers to the sRGB images downsampled $2 \times$ to match the resolution of the RAW images after extracting R, G, and B channels. We multiply Bleu and Regex scores by 10 to align them with the other metrics. Black lines indicate standard errors. The results show that captions generated from processed RAW images ($\log + \gamma$) achieve competitive quality, closely matching the reference captions.

RAWDET-7 dataset improves performance across individual datasets, compared to training the model individually with every subset. This indicates that combining multi-bit depth raw images during training helps the model generalize well on every subset of data, which further proves the usefulness of RAWDET-7.

5.3. Benchmarking Large VLMs (LVLMs)

We also benchmark RAWDET-7 on MM-Grounding-DINO for 4 quantization levels and various signal scaling techniques. Unfortunately, training or fine-tuning the VLM is computationally infeasible given our limited resources. Thus, we perform zero-shot evaluations while keeping the VLM frozen. However, scaling methods with γ require some training. Thus, for these, we keep the VLM frozen and only train the γ value with lr 1e-5 and a maximum training budget of 50 epochs. We observe that $\log + \gamma$ -SCALING performs the best, even exceeding the perfor-

mance on sRGB for some quantization levels. $\log + \gamma$ -SCALING highlights the details of the images in a better way as compared to other image-enhancing baselines. These results are promising, as they show that at multiple-quantization levels, even models trained on a very large amount of sRGB data is able to extract more information out from RAW image input than sRGB input, leading to better performance on RAW input after quantization level over 4-bit depth. Since at 6-bit depth itself RAW input to MM-Grounding-DINO outperforms sRGB input, we visualize qualitative results for 6-bit depth quantization in Fig. 5.

5.4. Object Description

Next, we study object description quality across different RAW preprocessing pipelines. Since current VLMs are closed and cannot be finetuned end-to-end on RAW, we adopt a zero-shot setting and reuse the γ values that previously yielded strong robustness in our object detection experiments across architectures and bit depths. For this analysis, we randomly sample 500 images from the RAWDET-7 validation set and treat high-resolution sRGB as our reference modality. Each image is annotated with set-of-marks and provided twice to Gemini-2.5-Pro [7] in order to probe the stability of its object descriptions on sRGB.

From the corresponding Bayer-patterned RAW measurements, we extract R, G, and B channels and construct two families of quantized RAW variants at 4, 6, and 8 bits: a linear mapping and a $\log + \gamma$ mapping that combines logarithmic compression with the reused γ values. In addition, we generate a $2 \times$ downsampled sRGB image whose effective resolution roughly matches that of the 8-bit RAW variants. All non-reference representations (downsampled sRGB, linear RAW, $\log + \gamma$ RAW) are overlaid with the same set-of-marks and passed to Gemini-2.5-Pro for object descriptions. Caption quality is then evaluated against the high-resolution sRGB baseline using five metrics: Bleu, Regex Match, Similarity (1-10), Detail Match (1-10), and Detail Level (1-10), with the last three obtained from Gemini-2.5-Flash-Lite for consistent qualitative scoring. Formal metric definitions are deferred to the appendix.

The results in Fig. 6 show a consistent pattern. Across all bit depths, linearly quantized RAW images produce captions that are less similar to the sRGB reference and clearly underperform in detail and detail match, indicating that naive RAW quantization discards semantically important structure. In contrast, $\log + \gamma$ quantized RAW images retain much more fine-grained information and achieve scores close to, and sometimes approaching, high-resolution sRGB, while the $2 \times$ downsampled sRGB variant sits between the two extremes. This supports our central claim that careful RAW preprocessing can already narrow the gap between what an RGB-pretrained VLM can describe on sRGB and on RAW inputs. At the same time, the

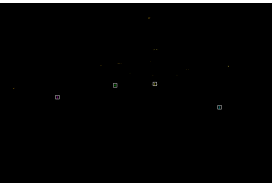
sRGB: Similarity 8.5 ± 0.58 Detail Level 5.0 ± 0.82 Detail Match 8.0 ± 0.82 	sRGB: Similarity 8.5 ± 0.71 Detail Level 4.5 ± 2.12 Detail Match 7.5 ± 0.71 
Linear 4-bits: Similarity 1.0 ± 0.00 Detail Level 0.0 ± 0.00 Detail Match 1.0 ± 0.00 	Linear 4-bits: Similarity 7.5 ± 2.12 Detail Level 2.5 ± 0.71 Detail Match 5.5 ± 4.95 
Log-γ 4-bits: Similarity 6.2 ± 2.99 Detail Level 5.8 ± 1.50 Detail Match 4.5 ± 3.00 	Log-γ 4-bits: Similarity 7.5 ± 0.71 Detail Level 7.0 ± 0.00 Detail Match 7.5 ± 0.71 

Figure 7. Comparison of caption quality for different image representations, including quantitative scores. Captions generated from Log- γ images provide more detail-level explanations compared to those from Linear 4-bit quantized images.

remaining gap and the strong sensitivity to preprocessing underline that bad RAW processing leads to systematically poorer descriptions, whereas good RAW-aware mappings are feasible and worth optimizing, as visualized in Fig. 7. The object description track in RAWDET-7 makes these trade-offs measurable and enables future work to benchmark RAW preprocessing pipelines, not only against sRGB, but also across multiple bit-depth-accurate RAW variants.

Looking forward, optimizing gamma specifically for image caption generation may further improve performance, potentially surpassing that of sRGB.

6. Conclusion

RAWDET-7 fills a critical gap in the vision community by enabling robust, efficient, and generalizable object detection directly on RAW sensor data. By unifying and re-annotating four existing datasets, we provide a diverse and high-quality corpus that spans a wide range of lighting conditions, environments, and sensor types. Our dense, consistent annotations across seven common object categories resolve the limitations of prior RAW datasets, including noisy labels, limited class coverage, and inconsistent naming conventions. Moreover, the addition of object captions makes it a useful tool for bridging low-level RAW image processing with high-level semantic understanding, enabling tasks like caption-guided detection on RAW data.

RAWDET-7 supports controlled benchmarking under various quantized inputs, reflecting practical constraints at the sensor level, such as reduced bandwidth and energy

consumption. We empirically demonstrate that training on RAWDET-7 leads to consistent performance improvements across standard detectors like Faster R-CNN, RetinaNet, and PAA. Moreover, we show that even a LVLM, MM-Grounding DINO, can make meaningful zero-shot predictions on quantized RAW inputs, particularly when simple input normalization strategies are applied. We anticipate that RAWDET-7 will serve as a catalyst for further research in low-level vision, quantization-aware modeling, and end-to-end co-design of sensors and modern vision systems.

Limitations. RAWDET-7 improves coverage of sensor settings by building on diverse prior datasets, but its coverage of the broader RAW sensor landscape remains limited. The dataset is also imbalanced across sensors and bit depths, with most images at 24-bit. Even if the practical impact is unclear, a more balanced sensor representation is desirable. In principle, additional RAW datasets could be merged into RAWDET-7 and annotated using our pipeline, but expanding annotations is costly because high-quality annotation tools (including ours) are paid.

Acknowledgements. The authors acknowledge support by the DFG Research Unit 5336 - Learning to Sense (L2S). We would also like to thank Penelope Natusch for her helps with the project. The authors gratefully acknowledge the computing time provided on the high-performance computer HoreKa by the National High-Performance Computing Center at KIT (NHR@KIT). We thank Janis Keuper for his support.

References

[1] Navya Sonal Agarwal, Jan Philipp Schneider, Kanchna Vaishnavi Gandikota, Syed Muhammad Kazim, John Meshreki, Ivo Ihrke, and Michael Moeller. Direct image classification from fourier ptychographic microscopy measurements without reconstruction, 2025. 1

[2] Shashank Agnihotri, Jonas Jakubassa, Priyam Dey, Sachin Goyal, Bernt Schiele, Venkatesh Babu Radhakrishnan, and Margret Keuper. A granular study of safety pretraining under model ablation. In *NeurIPS Workshop Lock-LLM Workshop: Prevent Unauthorized Knowledge Use from Large Language Models*, 2025. 10

[3] A. Bermak and A. Kitchen. A novel adaptive logarithmic digital pixel sensor. *IEEE Photonics Technology Letters*, 18(20):2147–2149, 2006. 5

[4] Mark Buckler, Suren Jayasuriya, and Adrian Sampson. Reconfiguring the imaging pipeline for computer vision. In *Proceedings of the IEEE International Conference on Computer Vision (ICCV)*, 2017. 2, 3, 5

[5] Mu Cai, Haotian Liu, Siva Karthik Mustikovela, Gregory P. Meyer, Yuning Chai, Dennis Park, and Yong Jae Lee. Making large multimodal models understand arbitrary visual prompts. In *IEEE Conference on Computer Vision and Pattern Recognition*, 2024. 3

[6] Kai Chen, Jiaqi Wang, and et al. Mmdetection: Open mmlab detection toolbox and benchmark, 2019. 5

[7] Gheorghe Comanici, Eric Bieber, Mike Schaeckermann, Ice Pasupat, Noveen Sachdeva, Inderjit Dhillon, Marcel Blissein, Ori Ram, Dan Zhang, Evan Rosen, et al. Gemini 2.5: Pushing the frontier with advanced reasoning, multimodality, long context, and next generation agentic capabilities. *arXiv preprint arXiv:2507.06261*, 2025. 4, 7

[8] Ziteng Cui and Tatsuya Harada. Raw-adapter: Adapting pre-trained visual model to camera raw images. In *European Conference on Computer Vision*, pages 37–56. Springer, 2024. 3

[9] Duc-Tien Dang-Nguyen, Cecilia Pasquini, Valentina Conotter, and Giulia Boato. Raise: A raw images dataset for digital image forensics. In *Proceedings of the 6th ACM multimedia systems conference*, pages 219–224, 2015. 3

[10] Steven Diamond, Vincent Sitzmann, Frank Julca-Aguilar, Stephen Boyd, Gordon Wetzstein, and Felix Heide. Dirty pixels: Towards end-to-end image processing and perception. *ACM Transactions on Graphics (TOG)*, 40(3):1–15, 2021. 3

[11] Mishal* Fatima, Shashank* Agnihotri, Marius* Bock, Kanchna Vaishnavi Gandikota, Kristof Van Laerhoven, Michael Moeller, and Margret Keuper. γ -Quant: Towards Learnable Quantization for Low-bit Pattern Recognition. *DAGM German Conference on Pattern Recognition*, 2025. 2

[12] Xavier Glorot, Antoine Bordes, and Yoshua Bengio. Deep sparse rectifier neural networks. In *Proceedings of the Fourteenth International Conference on Artificial Intelligence and Statistics*, pages 315–323, Fort Lauderdale, FL, USA, 2011. PMLR. 5

[13] Rahul Gulve, Navid Sarhangnejad, Gairik Dutta, Motasem Sakr, Don Nguyen, Roberto Rangel, Wenzheng Chen, Zhengfan Xia, Mian Wei, Nikita Gusev, Esther Y. H. Lin, Xiaonong Sun, Leo Hanxu, Nikola Katic, Ameer M. S. Abdellahi, Andreas Moshovos, Kiriakos N. Kutulakos, and Roman Genov. 39 000-subexposures/s dual-adc cmos image sensor with dual-tap coded-exposure pixels for single-shot hdr and 3-d computational imaging. *IEEE Journal of Solid-State Circuits*, 58(11):3150–3163, 2023. 5

[14] Agrim Gupta, Piotr Dollar, and Ross Girshick. LVIS: A dataset for large vocabulary instance segmentation. In *Proceedings of the IEEE Conference on Computer Vision and Pattern Recognition*, 2019. 1

[15] Kaiming He, Xiangyu Zhang, Shaoqing Ren, and Jian Sun. Deep residual learning for image recognition. In *Proceedings of the IEEE conference on computer vision and pattern recognition*, pages 770–778, 2016. 5

[16] Andrey Ignatov, Luc Van Gool, and Radu Timofte. Replacing mobile camera isp with a single deep learning model. In *Proceedings of the IEEE/CVF conference on computer vision and pattern recognition workshops*, pages 536–537, 2020. 1, 3, 4

[17] Kang Kim and Hee Seok Lee. Probabilistic anchor assignment with iou prediction for object detection. In *Computer Vision–ECCV 2020: 16th European Conference, Glasgow, UK, August 23–28, 2020, Proceedings, Part XXV 16*, pages 355–371. Springer, 2020. 3, 5

[18] Tzofi Klinghoffer, Siddharth Somasundaram, Kushagra Tiwary, and Ramesh Raskar. Physics vs. learned priors: Rethinking camera and algorithm design for task-specific imaging. In *2022 IEEE International Conference on Computational Photography (ICCP)*, pages 1–12. IEEE, 2022. 1

[19] Martin Lefebvre and David Bol. Mantis: A mixed-signal near-sensor convolutional imager soc using charge-domain 4b-weighted 5-to-84-tops/w mac operations for feature extraction and region-of-interest detection. *IEEE Journal of Solid-State Circuits*, 60(3):934–948, 2025. 5

[20] Xuanyu Lei, Zonghan Yang, Xinrui Chen, Peng Li, and Yang Liu. Scaffolding coordinates to promote vision-language coordination in large multi-modal models. In *Proceedings of the 31st International Conference on Computational Linguistics*, pages 2886–2903, Abu Dhabi, UAE, 2025. Association for Computational Linguistics. 3

[21] Zhihao Li, Ming Lu, Xu Zhang, Xin Feng, M. Salman Asif, and Zhan Ma. Efficient visual computing with camera raw snapshots. *IEEE Transactions on Pattern Analysis and Machine Intelligence*, 46(7):4684–4701, 2024. 3

[22] Zhihao Li, Ming Lu, Xu Zhang, Xin Feng, M Salman Asif, and Zhan Ma. Efficient visual computing with camera raw snapshots. *IEEE Transactions on Pattern Analysis and Machine Intelligence*, 46(7):4684–4701, 2024. 3

[23] Tsung-Yi Lin, Michael Maire, Serge Belongie, James Hays, Pietro Perona, Deva Ramanan, Piotr Dollár, and C Lawrence Zitnick. Microsoft coco: Common objects in context. In *Computer Vision–ECCV 2014: 13th European Conference, Zurich, Switzerland, September 6–12, 2014, Proceedings, Part V 13*, pages 740–755. Springer, 2014. 1

[24] Tsung-Yi Lin, Priya Goyal, Ross Girshick, Kaiming He, and Piotr Dollár. Focal loss for dense object detection. In *Pro-*

ceedings of the IEEE international conference on computer vision, pages 2980–2988, 2017. 3, 5

[25] Anqi Liu, Shiyi Mu, and Shugong Xu. A learnable color correction matrix for raw reconstruction. In *British Machine Vision Conference*, 2024. 3

[26] Shilong Liu, Zhaoyang Zeng, Tianhe Ren, Feng Li, Hao Zhang, Jie Yang, Qing Jiang, Chunyuan Li, Jianwei Yang, Hang Su, et al. Grounding dino: Marrying dino with grounded pre-training for open-set object detection. In *European Conference on Computer Vision*, pages 38–55. Springer, 2024. 4

[27] Ze Liu, Yutong Lin, Yue Cao, Han Hu, Yixuan Wei, Zheng Zhang, Stephen Lin, and Baining Guo. Swin transformer: Hierarchical vision transformer using shifted windows. In *Proc. of the IEEE/CVF International Conference on Computer Vision (ICCV)*, 2021. 6

[28] William Ljungbergh, Joakim Johnander, Christoffer Petersson, and Michael Felsberg. Raw or cooked? object detection on raw images. In *Scandinavian Conference on Image Analysis*, pages 374–385. Springer, 2023. 2, 3

[29] Igor Morawski, Yu-An Chen, Yu-Sheng Lin, Shusil Dangi, Kai He, and Winston H Hsu. Genisp: Neural isp for low-light machine cognition. In *Proceedings of the IEEE/CVF Conference on Computer Vision and Pattern Recognition*, pages 630–639, 2022. 1, 3, 4

[30] Ali Mosleh, Avinash Sharma, Emmanuel Onzon, Fahim Mannan, Nicolas Robidoux, and Felix Heide. Hardware-in-the-loop end-to-end optimization of camera image processing pipelines. In *Proceedings of the IEEE/CVF Conference on Computer Vision and Pattern Recognition*, pages 7529–7538, 2020. 3

[31] A Omid-Zohoor, D Ta, and B Murmann. Pascalraw: raw image database for object detection, 2014. 1, 3, 4, 5

[32] Shaoqing Ren, Kaiming He, Ross Girshick, and Jian Sun. Faster r-cnn: Towards real-time object detection with region proposal networks. *IEEE transactions on pattern analysis and machine intelligence*, 39(6):1137–1149, 2016. 3, 5

[33] Nicolas Robidoux, Luis E Garcia Capel, Dong-eun Seo, Avinash Sharma, Federico Ariza, and Felix Heide. End-to-end high dynamic range camera pipeline optimization. In *Proceedings of the IEEE/CVF Conference on Computer Vision and Pattern Recognition*, pages 6297–6307, 2021. 3

[34] Olga Russakovsky, Jia Deng, Hao Su, Jonathan Krause, Sanjeev Satheesh, Sean Ma, Zhiheng Huang, Andrej Karpathy, Aditya Khosla, Michael Bernstein, Alexander C. Berg, and Li Fei-Fei. ImageNet Large Scale Visual Recognition Challenge. *International Journal of Computer Vision (IJCV)*, 115(3):211–252, 2015. 5

[35] Eli Schwartz, Raja Giryes, and Alex M. Bronstein. Deepisp: Toward learning an end-to-end image processing pipeline. *IEEE Transactions on Image Processing*, 28(2):912–923, 2019. 3

[36] Hendrik Sommerhoff, Shashank Agnihotri, Mohamed Saleh, Michael Moeller, Margret Keuper, and Andreas Kolb. Differentiable sensor layouts for end-to-end learning of task-specific camera parameters. *arXiv preprint arXiv:2304.14736*, 2023. 1

[37] Ilya Sutskever, James Martens, George Dahl, and Geoffrey Hinton. On the importance of initialization and momentum in deep learning. In *Proceedings of the 30th International Conference on Machine Learning*, pages 1139–1147, Atlanta, Georgia, USA, 2013. PMLR. 5

[38] David Wan, Jaemin Cho, Elias Stengel-Eskin, and Mohit Bansal. Contrastive region guidance: Improving grounding in vision-language models without training. In *European Conference on Computer Vision*, pages 198–215. Springer, 2024. 3

[39] Zhenwei Wu, Xinfu Wang, Meng Jia, Minghao Liu, Chengxiu Sun, Chenyang Wu, and Jianping Wang. Dense object detection methods in raw uav imagery based on yolov8. *Scientific reports*, 14(1):18019, 2024. 3

[40] Ruikang Xu, Chang Chen, Jingyang Peng, Cheng Li, Yibin Huang, Fenglong Song, Youliang Yan, and Zhiwei Xiong. Toward raw object detection: A new benchmark and a new model. In *Proceedings of the IEEE/CVF Conference on Computer Vision and Pattern Recognition*, pages 13384–13393, 2023. 1, 3, 4, 5

[41] Jianwei Yang, Hao Zhang, Feng Li, Xueyan Zou, Chunyuan Li, and Jianfeng Gao. Set-of-mark prompting unleashes extraordinary visual grounding in gpt-4v, 2023. 3, 4

[42] Lingfeng Yang, Yueze Wang, Xiang Li, Xinlong Wang, and Jian Yang. Fine-grained visual prompting. *Advances in Neural Information Processing Systems*, 36:24993–25006, 2023. 3

[43] Zhaoyang Yin, Yibing M. Wang, and Eric R. Fossum. Low bit-depth adcs for multi-bit quanta image sensors. *IEEE Journal of Solid-State Circuits*, 56(3):950–960, 2021. 2, 4

[44] Yin Zhang, Yongqiang Zhang, Zian Zhang, Man Zhang, Rui Tian, and Mingli Ding. Isp-teacher: Image signal process with disentanglement regularization for unsupervised domain adaptive dark object detection. In *Proceedings of the AAAI Conference on Artificial Intelligence*, pages 7387–7395, 2024. 3

[45] Xiangyu Zhao, Yicheng Chen, Shilin Xu, Xiangtai Li, Xinqiang Wang, Yining Li, and Haian Huang. An open and comprehensive pipeline for unified object grounding and detection. *arXiv preprint arXiv:2401.02361*, 2024. 3, 6

RAWDET-7: A Multi-Scenario Benchmark for Object Detection and Description on Quantized RAW Images

Supplementary Material

A Experimental Details	1
A.1 Object Detection Training Details	1
A.2 Details of Foundation Model used for Annotations	1
B User Study Comparing Our New Object Detection Annotations to Old	1
C Visualizing And Comparing Annotations From RAWDET-7	2
D Additional Dataset Statistics	4
E Additional Benchmarking Details e.g. details on the ISP used for RAW RGB conversion of the images from the RAOD dataset.	4
F. Advantage of Consolidated Dataset	4
G Object Descriptions	5
G.1 Generating Object Descriptions	5
G.2 User Study to Validate Quality of the Object Descriptions	7
G.3 Metrics for Evaluating Object Descriptions	7
G.4 User Study to Verify LLM as a Judge for Metrics	10

A. Experimental Details

Following, we provide more details regarding the object detection experimental setup: training details for the architecture and details on using the foundation model for generating the new annotations for RAWDET-7.

A.1. Object Detection Training Details

Following previous works, for training traditional object detection models, we follow multi-scale training where the shorter image side is scaled to one of the sides randomly selected from a set of sides: [480, 512, 544, 576, 608, 640, 672, 704, 736, 768, 800] using nearest neighbor interpolation and the longer side is scaled to maintain the aspect ratio. We apply a warm-up for the first 1000 iterations, linearly increasing the learning rate (lr) from $1e^{-3}$ to $2.5e^{-3}$ followed by a multi-step learning rate scheduler.

A.2. Details of Foundation Model used for Annotations

We used the paid API version at: https://deepdataspace.com/request_api. We use their model “Detection-Model.GDino1_5_Pro” for generating the bounding boxes and classes such that we only annotate objects with 20% or less overlap with another object of the same class (following recommended settings). The text prompt we used for generating the annotations was “car . truck . tram . person . bicycle . motorcycle . bus .”. Each query to the API costs ¥0.1, thus, including the debugging and ablations over prompts and classes, the total cost was ¥3402.80. Finally, after obtaining the annotations, we observed that the model was often hallucinating low-confidence objects. Thus, we filter out these hallucinated objects, after carefully observing multiple annotations and confidences, by using a confidence score threshold of 0.8, i.e. only annotations with confidence scores of 0.8 and above were retained, and the remaining were filtered out.

B. User Study Comparing Our New Object Detection Annotations to Old

We did a user survey for our new data annotations and received 53 responses. For the survey, we collected 100 random pairs of annotations such that for each image chosen at random, we had the annotation from RAWDET-7 and the annotation provided by the original dataset. We split the 100 random pairs of annotations into 4 sets of 25 questions each. Each question

22. Which annotations look more accurate? Please compare the two annotated images and select the one you believe has better object annotations. Consider accuracy, completeness, and correct labeling. In case both are bad, please select the one that you deem more acceptable for the scene. (Set 3, Q22)



Option A



Option B

23. Which annotations look more accurate? Please compare the two annotated images and select the one you believe has better object annotations. Consider accuracy, completeness, and correct labeling. In case both are bad, please select the one that you deem more acceptable for the scene. (Set 3, Q23)



Option A



Option B

Figure 8. Examples from the annotation-quality user study, where participants inspected bounding boxes and compared newly generated annotations against older versions to assess improvements in quality.

shuffled the order of option A and option B, with annotation from RAWDET-7 for that image being either option A or option B, and the other option being the annotation from the original dataset.

Given 25 questions to each user, and since 53 users responded, we had exactly 1325 instances of comparisons between the RAWDET-7 annotations and the original annotations answered. From these 1325 instances, users preferred the RAWDET-7 annotations in 1002 instances. That is, **users preferred RAWDET-7 annotations for 75.62% of all the instances**. This clearly demonstrates the improvement of the annotations provided by RAWDET-7. For ease of access to the comparisons, in Section C, we extended the comparison from Figure 1 and show a few examples comparing the annotations from RAWDET-7 and the original annotations.

Limitations Of The User Study. Post the study, a few users informed that they had to zoom in quite a bit to confirm that one annotation is better than the other. We suspect that the annotations that required zooming in were the annotations from RAWDET-7 since it provides very fine-grained detections as well. Users reported that, in a few instances, those who are not vigilant may not choose the RAWDET-7 annotations, and thus the final scores might underrepresent the benefit of the annotations from RAWDET-7.

C. Visualizing And Comparing Annotations From RAWDET-7

In Figure 9, we observe that RAWDET-7 covers many small objects in the images that were originally missing from the annotations, and correctly labels many misclassified objects in the original annotations.

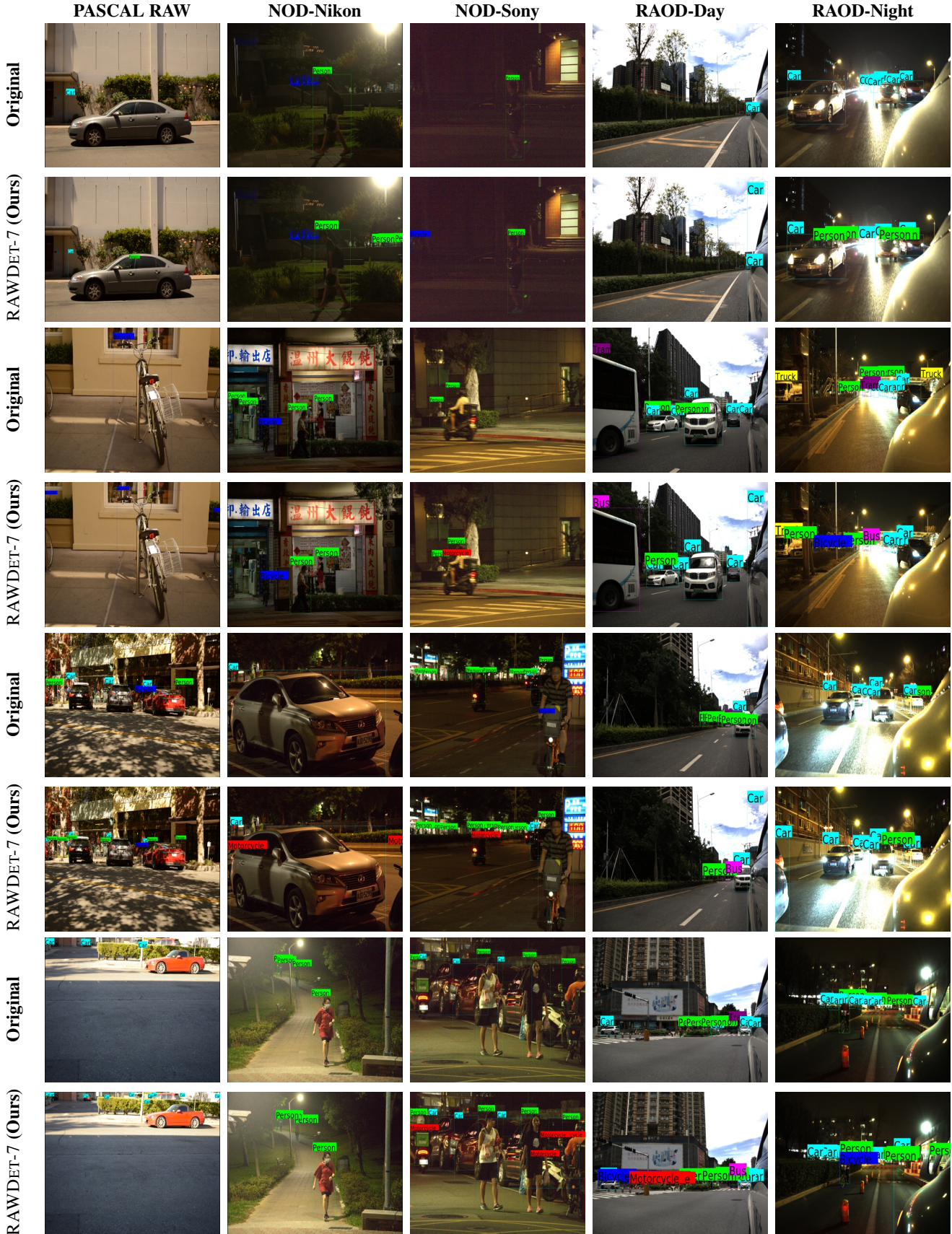


Figure 9. Comparing ground truth annotations provided in the original datasets and the new ones proposed in RAWDET-7 as used in the user study. Please note that the visualizations here are heavily compressed due to size limitations.

Table 3. Characteristics of Annotated Objects in RAWDET-7.

	Bicycle	Bus	Car	Motorcycle	Person	Tram	Truck
Avg. Obj Size (H × W)	477 × 431	224 × 301	250 × 257	231 × 195	508 × 213	177 × 307	231 × 257
Avg. Obj Count/Image	1.95	1.28	7.63	2.12	3.62	1.12	1.53
Avg. Aspect Ratio	0.939	1.486	1.350	0.888	0.528	2.192	1.197

Table 4. Characteristics of Different Datasets in RAWDET-7.

	Pascal Raw	Zurich	Raw-NOD-Nikon	Raw-NOD-Sony	RAOD
Sensor Model	Nikon D3200 DSLR	MP Sony Exmor IMX380	Nikon D750	Sony RX100 VII	Sony IMX490
Resolution	6034 × 4012	2944 x 3958	3968 × 2640	4256 × 2848	2880 × 1856
Bit Depth	12	10	14	14	24
Scenarios	Day	Day	Night	Night	Day and Night

D. Additional Dataset Statistics

In [Table 3](#), we list different object characteristics in the proposed RAWDET-7 dataset. Average object size is computed by averaging the height and width of bounding boxes across all images in the train and validation sets for a particular category. We observe that the bicycle category has the largest object size, and the motorcycle, truck, and tram have the smallest. The category "car" has the highest average object count per image, which is intuitive due to the outdoor nature of the proposed dataset. Average aspect ratio is computed by calculating the aspect ratio (width/height) of every object in a category and averaging over the entire dataset.

E. Additional Benchmarking Details e.g. details on the ISP used for RAW RGB conversion of the images from the RAOD dataset.

Except for the Zurich Dataset, the remaining individual datasets have a Bayer pattern of RGGB, whereas Zurich raw images have an RGBG pattern. We extract red, green, and blue channels from the relevant Bayer pattern and take the mean of the double green channels. For quantization experiments, we use `torch.floor` as a quantization function. In the case of gamma scaling, we use a straight-through estimator to let the gradients pass through the quantization operation. The RGB images of all the individual datasets are publicly provided along with the raw images, except for the RAOD dataset. So, we generated them by first extracting the Red, Green, and Blue channels from the original raw image, followed by a gray world white balance algorithm. Then, we apply gamma correction, where the value of gamma is chosen by hit-and-run to be 0.09.

F. Advantage of Consolidated Dataset

We show the advantage of adding all the individual datasets together for training vs. training only with the individual datasets in [Figure 10](#) for PAA architecture. We observe that while training with linear quantization without any scaling results in no performance gain when trained in a combined fashion, gamma scaling and RGB experiments usually benefit from combined training. This is especially visible in the case of the Sony and Nikon Datasets.

In [Figure 11](#), we show results with FRCNN for training on combined RAWDET-7 when evaluated on each subset, vs. training only on a subset and evaluated on the subset's test set. Combining improves results on the majority of the subsets in the case of gamma scaling and sRGB. These comparisons include all metrics (mAP, AP50, AP75) and cover 4, 6, and 8-bit depth data as well as sRGB.

In [Figure 12](#), we show precision-recall curves for the RAOD dataset. "Old" refers to the annotations as proposed in the original dataset, whereas "New" refers to the annotations in RAWDET-7. All the models are FasterRCNNs, trained for 8-bit quantization and jointly learnt with 1 gamma. As mentioned in the legend, the keys are "(Train Dataset - Evaluation Dataset)". Curves are shown for the classes car, truck, tram, and person.

In [Table 4](#), we summarize the statistics on the different datasets that we consolidate into RAWDET-7. The individual datasets have each a particular sensor model and bit depth. The combined dataset, therefore, provides significantly increased data diversity.

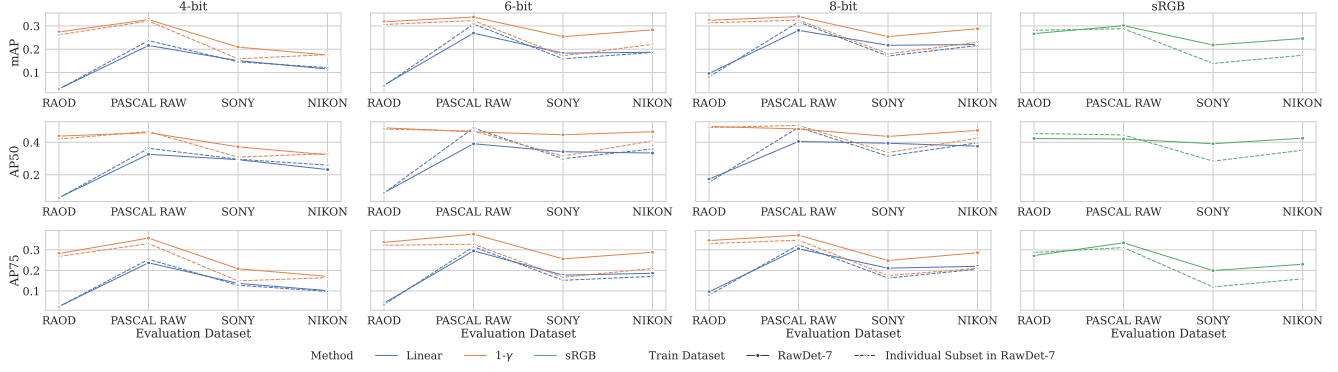


Figure 10. Results with PAA for training on combined RAWDET-7 when evaluated on each subset, vs. training only on a subset and evaluated on the subset’s test set. Combining improves results on the majority of the subsets in the case of gamma scaling and sRGB. These comparisons include all metrics (mAP, AP50, AP75) and cover 4, 6, and 8-bit depth data as well as sRGB.

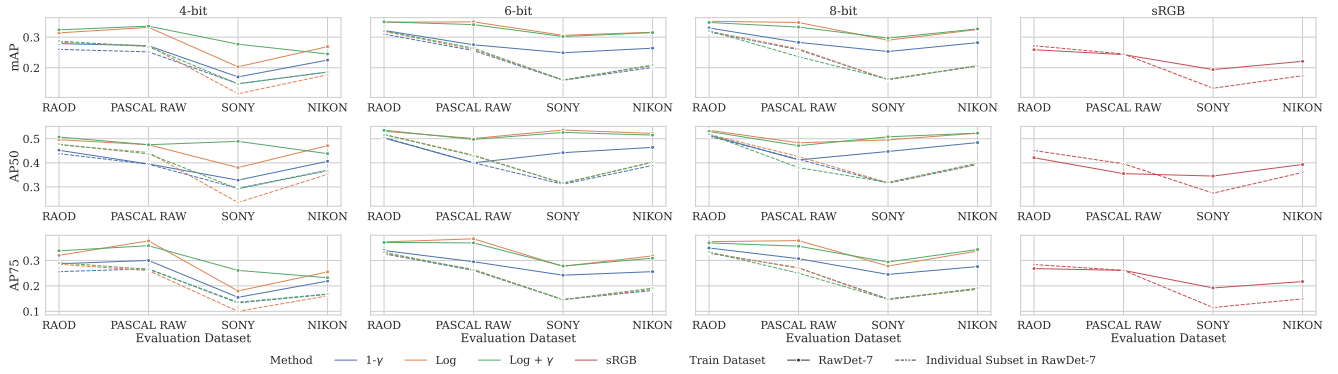


Figure 11. Results with FRCNN for training on combined RAWDET-7 when evaluated on each subset, vs. training only on a subset and evaluated on the subset’s test set. Combining improves results on the majority of the subsets in the case of gamma scaling and sRGB. These comparisons include all metrics (mAP, AP50, AP75) and cover 4, 6, and 8-bit depth data as well as sRGB.

In Figure 13, we provide detailed dataset statistics. In particular, we report statistics on instances in the original proposed datasets indicated by ‘OLD’ and the re-annotated images for those respective datasets indicated by ‘NEW’ for the classes in RAWDET-7. The proposed RAWDET-7 is a consolidation of RAW input images from the ‘OLD’ datasets provided with the ‘NEW’ annotations. For some classes, it appears that ‘OLD RAOD’ has more instances than the proposed RAWDET-7. Note that ROAD has a large number of objects annotated. However, as shown in Figure 1, the original annotations of the RAOD dataset contain hallucinations for classes like ‘Tram’, ‘Truck’, and ‘Car’.

The consolidated dataset RAWDET-7 provides cleaned labels for the diverse RAW data samples.

G. Object Descriptions

G.1. Generating Object Descriptions

For object captioning, we use the caption prompt used for object-level descriptions prompt with Gemini-2.5-Pro. The model receives the overlaid image where each detected object is marked with a numbered square, together with the list of corresponding class labels. The prompt enforces a strict line-based output format of the form “<number>: <caption>” and requires exactly one caption per numbered object, in order from 1 to N. We call Gemini-2.5-Pro on each marked image (twice for the sRGB reference and once for each RAW or RGB-downsampled variant) and then parse the returned text using a regular expression to obtain a dictionary that maps object indices to their captions, which is then used for both analysis and visualization.

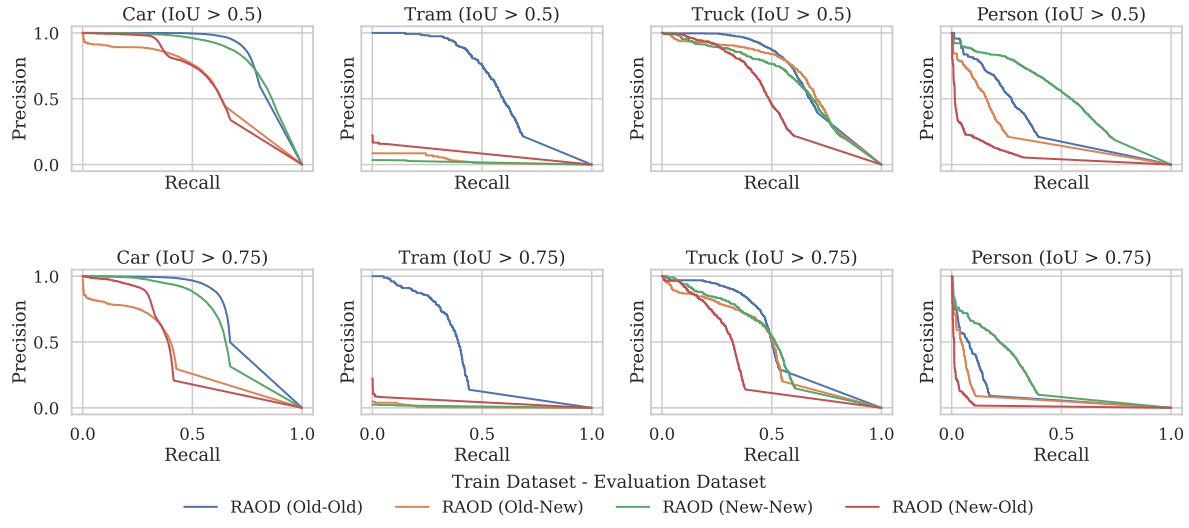


Figure 12. Precision Recall Curves for RAOD. “Old” refers to the annotations as proposed in the original dataset, whereas “New” means the annotations in RAWDET-7. All the models are trained on FasterRCNN for 8-bit quantization and jointly learnt with 1 gamma. As mentioned in the legend, the keys are “(Train Dataset - Evaluation Dataset)”. Curves are shown for the classes car, truck, tram, and person.

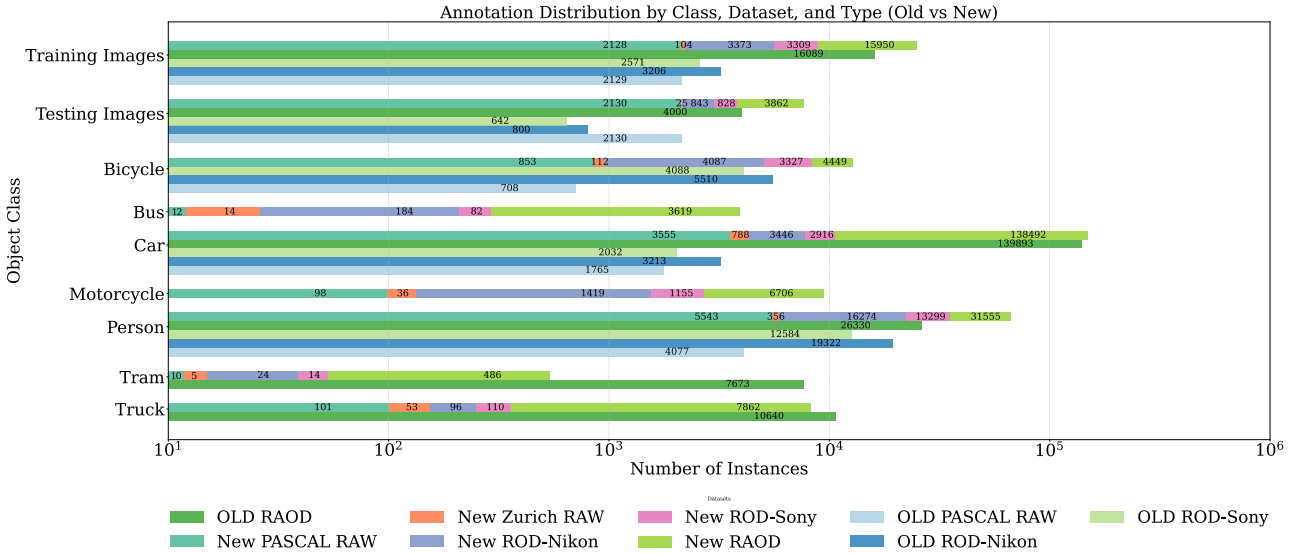


Figure 13. Dataset Statistics: Breakdown of instances in the original proposed datasets indicated by ‘OLD’ and the re-annotated images for those respective datasets indicated by ‘NEW’ for the classes in RAWDET-7. The proposed RAWDET-7 is a consolidation of RAW input images from the ‘OLD’ datasets provided with the ‘NEW’ annotations. For some classes, it appears that ‘OLD RAOD’ has more instances than the proposed RAWDET-7. However, as shown in Fig. 1, the original annotations of the RAOD dataset contain hallucinations for classes like ‘Tram’, ‘Truck’, and ‘Car’.

G.1.1. Prompts for Generating Object Descriptions

Caption prompt used for object-level descriptions

You will be shown a photo with multiple objects with these 7 classes of interest: cars, truck, tram, person, bicycle, motorcycle, bus.

Each object of interest is marked by a black square containing a coloured number.

Task: For EACH object with a marked number, produce ONE detailed, factual caption that ONLY describes that numbered object.

Include concrete details when visible: color, material/texture, approximate size class, local position (e.g., top-left), distinctive parts, visible text/markings, and immediate context relations.

STRICT OUTPUT:

Write ONE line per object using this exact pattern: <number>: <caption>

Acceptable separators after the number are ':', ')', '.', or '-' (e.g., '1: ...' or '1 ...').

Do NOT include headings, bullets, blank lines, or any extra text before/after the list.

If a numbered object cannot be seen or identified, write exactly: 'I cannot see the object'.

The numbering starts at 1 and goes up to N, where N is the total number of marked objects in the image.

There should be exactly N lines in your output, one for each numbered object.

If N is the highest number visible, ensure you include captions for all numbers from 1 to N in order.

We will tell you the object class of each marked object in the following way:

1: <CLASS>

2: <CLASS>

...

N: <CLASS>

If a numbered mark itself cannot be seen or identified in the image, write exactly: 'I cannot see the mark'.

DO NOT HALLUCINATE ANY MARKED NUMBERS.

DO NOT TALK ABOUT THE MARK SQUARES OR NUMBERS ITSELF or the WHOLE IMAGE.

G.2. User Study to Validate Quality of the Object Descriptions

We conducted a user study to evaluate the effectiveness of generated captions. We selected 100 images with the highest mean detail levels and then randomly sampled 20 images and their respective captions from these for each user study. We chose the 100 images with the highest mean detail level, since usually it is the longer output text where generative models hallucinate the most, as they often try to make up details. We wanted the user study to validate that this is not the case in our proposed object descriptions. Participants were shown each image along with its captions and asked to rate the quality of the captions on how well they described the marked objects in each image on a scale from 0 to 5. Here, 0 meant that the object description does not describe the object at all, and 5 meant that the object description describes the respective marked object reasonably well, leaving out almost no describable visual cues.

A total of 63 users participated in this study, so a total of 63×20 , that is, 1260 samples were collected for the quality of the captions. We received an average rating of $\frac{4.07 \pm 0.48}{5}$, that is $\approx 82\%$ score, which demonstrates the good quality of the object descriptions generated.

G.3. Metrics for Evaluating Object Descriptions

- **BLEU:** Measures how much the generated text overlaps in wording with a reference.
- **Regex Match:** Checks if the output matches a specific pattern or format.
- **Similarity (1–10):** Rates how semantically similar the meaning of two texts are, irrespective of the specific details.

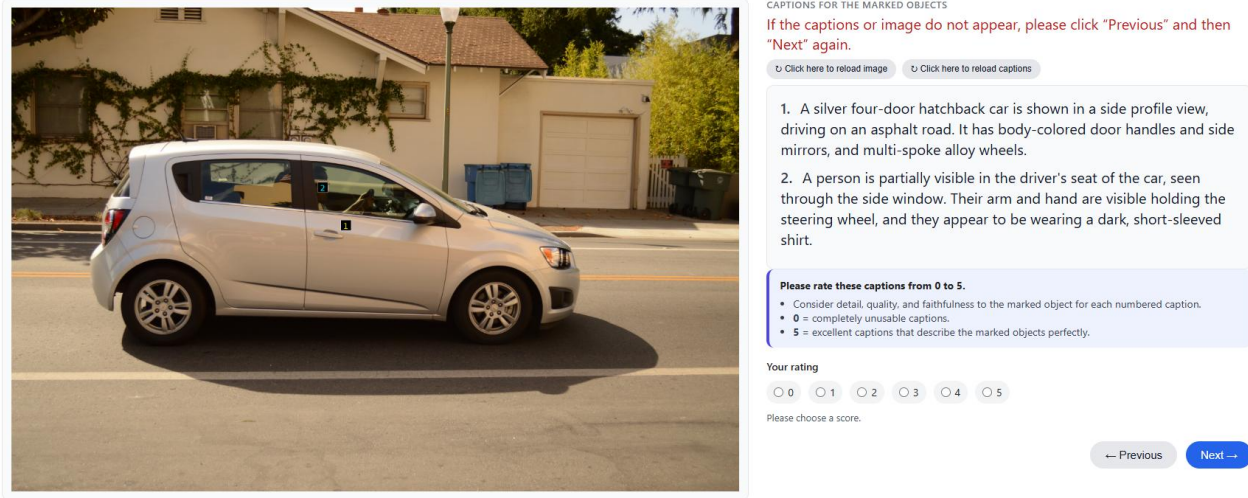


Figure 14. Example from the user study used to assess caption quality. Participants were shown images with designated markers and asked to rate the quality of the accompanying captions, where 0 is completely unusable and 5 is fully descriptive, clear, and highly informative.

- **Detail Level (0–10):** Rates how much detail or specificity the output contains.
- **Detail Match (1–10):** Rates how well specific details in the output match the reference.

Similarity. To quantify semantic similarity between two captions that describe the same object, we use the *Similarity* scoring prompt with Gemini-2.5-Flash-Lite. This prompt presents Caption A and Caption B and instructs the model to ignore surface-level differences such as wording (for example, “car” versus “sedan”) and colour or brightness variations, and to focus instead on whether both captions refer to the same underlying object with consistent meaning. The model is required to output a single integer in [1, 10] on a separate line, where 1 denotes unrelated or contradictory descriptions and 10 denotes near-identical semantics. We use this score as the *Similarity* metric for each caption pair, where one of the captions is always the first caption generated for the full-scale RGB image.

Detail Level. To assess how informative a single caption is, we use the *Detail level* prompt with Gemini-2.5-Flash-Lite. The prompt asks the model to rate the richness of grounded detail in one caption only, again returning a single integer score in [0, 10]. The instructions explicitly direct the model to base its judgment on concrete attributes such as materials, positions, parts, readable text, and local relations, while ignoring fluency and style. A score of 0 indicates no grounded detail, whereas 10 corresponds to a very specific, highly descriptive caption. We treat this as the *Detail Level* metric and compute it for each caption that we evaluate.

Detail Match. Finally, we measure the consistency of fine-grained information between two captions using the *Detail match* prompt, again with Gemini-2.5-Flash-Lite. Here, Caption A (first full-scale sRGB caption) acts as the reference and Caption B as the candidate, and the model is instructed to assign a score in [1, 10] based on the overlap of concrete, verifiable details such as materials, positions, parts, readable text and relations, while explicitly disregarding differences in colours or brightness due to varying image processing. Low scores correspond to almost no shared details, whereas scores near 10 indicate high overlap in grounded content. This yields the *Detail Match* metric, which we aggregate over objects and variants to analyze how well different pipelines preserve detailed object-level information.

G.3.1. Prompts for LLM as a Judge

Similarity scoring prompt

You are scoring the semantic similarity between two captions that describe the **SAME** object.

Check if they are roughly talking about the same object, ignore details.

Disregard similarity in colour, and disregard difference in brightness of the colours; disregard the exact word used, for example, car or sedan; focus on overall meaning match.

Return **ONLY** one integer in [1,10] on a single line with no other text.

Scoring: 1=unrelated/contradictory, 10=near-identical meaning (paraphrases penalize contradictions).

Be strict about the overall meaning match.

Caption A:

{A}

Caption B:

{B}

Detail level prompt

You are scoring the richness of a **SINGLE** caption, that is, how long and detailed and descriptive it is.

Return **ONLY** one integer in [0,10] on a single line with no other text.

Score based on concrete grounded attributes (colors, materials, positions, parts, readable text, relations).

Be strict about verifiable details only. 10=very rich and specific, 0=no grounded detail

.

Do not look for the length of the caption, only the amount of concrete details.

Ignore fluency/style. 0=no grounded detail, 10=very rich and specific.

Caption:

{C}

Detail match prompt

You are scoring the overlap of concrete details between two captions.

Return **ONLY** one integer in [1,10] on a single line with no other text.

Score high only if both share consistent verifiable details (materials, positions, parts, readable text, relations).

Disregard colour differences, and difference in brightness of the colours as the images are processed differently, and colour differences are expected, so disregard them.

Ignore fluency/style. 1=no shared details, 10=high detail overlap.

Be strict about concrete detail match.

Caption A:

{A}

Caption B:

{B}

G.4. User Study to Verify LLM as a Judge for Metrics

In order to validate the usage of LLMs as a judge to measure description similarity and level of detail, we also conducted a user study. [Figure 15](#) provides an example from this user study. We gather a random subset of 50 images with the two object descriptions per marked object in the images, gathered from the high-resolution sRGB version of each image, and ask users to provide scores between 0 and 10 for the description similarity, the amount of details provided, and the agreement of the given details.

Each user rates 10 of the 50 randomly sampled images at a time. We collected 9 such user studies, so 90 images and their respective pair of object descriptions for each marked object were rated, that is, a total of 391 caption pairs. We calculate the correlation in the mean similarity, mean detail level, and mean detail match between Gemini-2.5-Flash-Lite as a judge and a human as a judge from each user study. For similarity, we get a correlation of 0.61, for the detail level, we get a correlation of 0.71, and for the detail match, we get a correlation of 0.58. There are all high positive correlations, demonstrating that Gemini-2.5-Flash-Lite can be used as a judge for comparing two object descriptions at a time. Please note, using a better LLM like ChatGPT5 or Gemini-2.5-Pro as a judge might lead to better correlations with humans as a judge; however, this would incur high costs, and thus using Gemini-2.5-Flash-Lite is the most cost-effective way. Using open-source models for LLM as a judge might seem like a reasonable choice; however, as shown by [\[2\]](#), open-source models like Qwen3, GPT-oss have significantly low correlation with human judgment compared to closed and paid models.

The specific instructions given to the user, for “human as a judge” are:

Thank you for taking part in this study. In each trial you will see a high-resolution image with numbered marks on several objects. For every numbered object there are two automatically generated captions that are intended to describe the same marked object.
Your task is to rate the relationship between the two captions for each numbered object. For every object number, you will provide one visibility judgment and four scores on a scale from 0 to 10:

- Is the marked object actually visible? (Dependent on the image) Decide whether the object with this number is fully visible in the image, only partially visible, or not visible at all.
- Semantic similarity (Independent of the image) - Do both captions clearly talk about the same object, ignoring fine-grained detail.
- Level of detail of Caption 1 (Independent of the image) - How rich and specific Caption 1 is, in terms of concrete, verifiable details (independent of the image, verifying if the caption itself has obvious conflicts in the text).
- Level of detail of Caption 2 (Independent of the image) - Same as above, now for Caption 2.
- Detail match (Independent of the image) - How well the concrete details in Caption 1 and Caption 2 agree with each other.

Rating scale (0 to 10)

- 0 - No similarity or no grounded details at all.
- 5 - Moderate similarity or a moderate amount of grounded details.
- 10 - Very high similarity or very rich and specific grounded details.

The 0 to 10 scale applies to the four numeric scores. The visibility question instead uses the options Yes, No, and Only partially.

Only for the visibility question (Is the marked object actually visible?), you should look at the image. For all other scores, please ignore the image itself and judge only the two captions for that object. If a caption contains many details that are internally inconsistent or impossible (for example, mentioning both headlights and taillights when only the front of a car can be visible), please give low scores for the relevant detail and detail-match questions.

Please pay attention that each caption is tied to a numbered object in the image. When you score, always think about the object with that number, not the whole image.

IMAGE 8 OF 10



CAPTION PAIRS FOR THE NUMBERED OBJECTS

If the image or captions do not appear, please click "Previous" and then "Next" again. The next images and captions are preloaded in the background, but slow connections can still cause hiccups.

[Click here to reload image](#)

[Click here to reload captions](#)

OBJECT 1 – CAPTION 1

A person with dark hair, wearing a red short-sleeved shirt and dark shorts, is riding a bicycle at night while carrying a dark backpack.

OBJECT 1 – CAPTION 2

A person wearing a red short-sleeved shirt, dark shorts, and a dark backpack, seen in profile while riding a bicycle from left to right.

SCORES

Similarity	<input type="text"/>	<input type="button" value="▼"/>
Detail C1	<input type="text"/>	<input type="button" value="▼"/>
Detail C2	<input type="text"/>	<input type="button" value="▼"/>
Detail match	<input type="text"/>	<input type="button" value="▼"/>
Is the marked object actually visible?	<input type="text"/>	<input type="button" value="▼"/>

OBJECT 2 – CAPTION 1

A light-colored step-through frame bicycle with a basket on the front is being ridden on an asphalt road at night.

OBJECT 2 – CAPTION 2

A light-colored, step-through frame bicycle with a dark basket on the front, being ridden at night on an asphalt road.

SCORES

Similarity	<input type="text"/>	<input type="button" value="▼"/>
Detail C1	<input type="text"/>	<input type="button" value="▼"/>
Detail C2	<input type="text"/>	<input type="button" value="▼"/>
Detail match	<input type="text"/>	<input type="button" value="▼"/>
Is the marked object actually visible?	<input type="text"/>	<input type="button" value="▼"/>

For each object number, please answer all questions.

- Is the marked object actually visible? Choose Yes, No, or Only partially, based on the image.
- Similarity looks only at overall meaning of the two captions, ignore fine detail and ignore the image.
- Detail level looks at grounded, verifiable details in each caption separately, again ignoring the image.
- Detail match looks at how strongly the concrete details overlap between the two captions.

The four numeric scores use a scale from 0 (very low) to 10 (very high). If a caption contains many details that are inconsistent or impossible, please give low detail or detail-match scores.

[Previous image](#)

[Next image](#)

Figure 15. User-study example used to evaluate the performance of an LLM acting as a judge. Participants rated captions based on similarity with one another and richness of details. To assess the captioning model’s hallucinations, they also indicated whether the objects described were visible in the images or not.